Bow Shock Formation in a Complex Plasma

Y. Saitou,[1] Y. Nakamura,[2] T. Kamimura,[3] and O. Ishihara[2]

[1]*Faculty of Engineering, Utsunomiya University, Utsunomiya 321-8585, Japan*
[2]*Faculty of Engineering, Yokohama National University, Yokohama 240-8501, Japan*
[3]*Faculty of Science and Technology, Meijo University, Nagoya 468-8502, Japan*

(Received 13 August 2011; published 10 February 2012)

A bow shock is observed in a two-dimensional supersonic flow of charged microparticles in a complex plasma. A thin conducting needle is used to make a potential barrier as an obstacle for the particle flow in the complex plasma. The flow is generated and the flow velocity is controlled by changing a tilt angle of the device under the gravitational force. A void, microparticle-free region, is formed around the potential barrier surrounding the obstacle. The flow is bent around the leading edge of the void and forms an arcuate structure when the flow is supersonic. The structure is characterized by the bow shock as confirmed by a polytropic hydrodynamic theory as well as numerical simulation.

DOI: 10.1103/PhysRevLett.108.065004 PACS numbers: 52.27.Lw, 47.40.Ki, 52.30.−q, 52.35.Tc

A shock wave is a universal phenomenon observed in various media [1–8]. In particular, a bow shock is one of such shock waves as observed through the interaction of the magnetic field of Earth and the solar wind [8]. A void, where microparticles are excluded, is formed in a complex plasma under microgravity or by inserting a probe. Surrounding the boundary of the void, some interesting phenomena have been found and studied [9–11]. Thompson *et al.* have reported on interactions of a metal object and charged microparticles by moving the object in a dusty plasma with velocities faster and slower than the dust acoustic velocity [12]. Complex plasmas have become a useful tool to study fundamental aspects of physics by providing the opportunity to observe the phenomena involving microparticles by naked eyes [13,14].

In this Letter, we report the experimental observation of a two-dimensional bow shock formation in a large area two-dimensional complex plasma system with a supersonic flow of charged microparticles interacting with a stationary object. The observed bow shock structure is compared with theory and a molecular dynamics simulation.

The experiments were performed using the YCOPEX (Yokohama Complex Plasma Experiment) device [15] with modifications as shown in Fig. 1. The maximum experimental area of the device is 800 mm in length and 120 mm in width. An up-and-down gate separated the metal plate into two regions: the left region being the reservoir of the microparticles and the right one being the experimental region. Microparticles were supplied from a dust source at the left edge of the metal plate. The supplied microparticles were prevented from flowing with the raised gate even when the device was tilted toward the obstacle. By tilting the entire device with a jack and lowering the gate, a flow of charged microparticles was permitted. Although we arbitrarily set the potentials, the gate and the metal plate in the present case were electrically grounded. The gate was located at $x = -370$ [mm] from the obstacle. The obstacle, which was a conducting thin wire of 0.2 mm in diameter and 25 mm in length, was placed at $(x, y) = (0, 0)$ [mm], where x is parallel and y is vertical to the flow direction in the metal plate. The potential of the obstacle was floating and was −30 V against the plasma potential.

The base vacuum pressure was less than 0.4 Pa and argon gas pressure was 3.6 Pa. To avoid the drag of neutral particles or of the ions [15–18], the vacuum pump and the gas feeding were stopped when the pressure reached the value. A liquid nitrogen trap placed between the tube and the pump was filled with liquid nitrogen. Plasma was generated with an rf discharge of 5 W (13.56 MHz). The shape of the rf antenna was changed from a pair of parallel

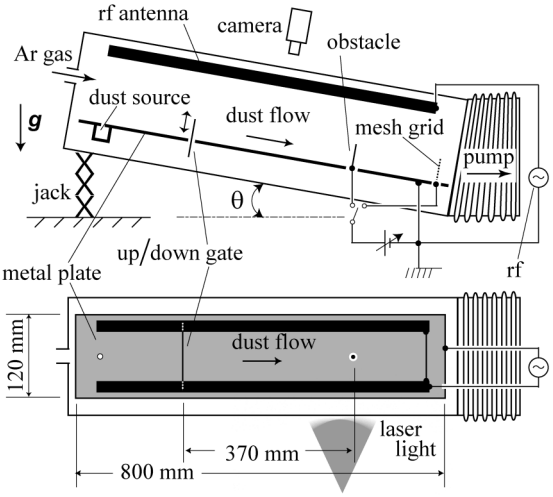

FIG. 1. Schematic drawing of the experimental glass chamber YCOPEX device. The side view (above) shows the tilted chamber and the top view (below) shows the reservoir region of microparticles in the left of the gate and the experimental region in the right of the gate.

ring antennas of the prototype YCOPEX to a parallel one to make the plasma uniform even when its volume became larger. The measured plasma parameters were $n_e \sim 5 \times 10^{14}$ [m^{-3}], $T_e \sim 5$ [eV], and the plasma potential was 30 V.

The microparticles were Au coated silica spheres with 5 μm in diameter and $m_d = 1.68 \times 10^{-13}$ [kg] in mass. The particles were charged to $Q = Z_d e = -(4.4 \pm 0.5) \times 10^4 e$, where e is the elementary electric charge [18]. The particles levitated approximately 8 mm above the metal plate. The region is known as the transient sheath [19]. The microparticles formed thin layers in the experimental region and the flow of the microparticles can be regarded almost to be two dimensional. The microparticles were irradiated with two thin fan green laser lights from the radial directions. Scattered laser light from the particles was observed and recorded with a camera placed outside above the device.

The velocity of a wave excited in the dusty plasma, C_d, was measured using the time-of-flight method with the tilt angle, θ, fixed at 0°. A pulsed voltage (~ -30 V) was applied to a mesh grid placed at the right edge of the plate. The applied negative voltage to the mesh grid changes the sheath potential profile in front of the grid and excites a burstlike phenomenon such as a pseudowave. The velocity was measured 5 cm away from the grid to avoid such a burstlike effect affecting the measurements. The result of the experiment is shown in Fig. 2. It is known that there are several longitudinal wave modes in complex plasmas. Typically, one is the dust acoustic (DA) mode, and the other is the dust lattice (DL) mode. The DA wave velocity, C_{DA}, and the DL velocity, C_{DL}, are given by

$$C_d = u(Z_d, m_d) f(\kappa) \tag{1}$$

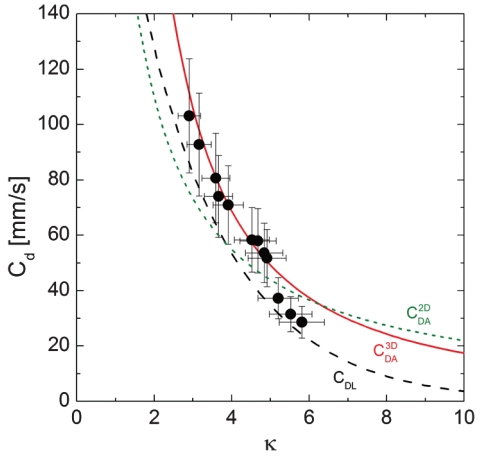

FIG. 2 (color online). Wave velocity C_d as a function of screening parameter κ. Measured values (solid circles) are compared with three-dimensional and two-dimensional dust acoustic velocities ($C_{\mathrm{DA}}^{\mathrm{3D}}$, solid line and $C_{\mathrm{DA}}^{\mathrm{2D}}$, dotted line) and dust lattice velocity (C_{DL}, dashed line).

where

$$u(Z_d, m_d) = \sqrt{\frac{{Z_d}^2 e^2}{\varepsilon_0 m_d \lambda_{\mathrm{Di}}}}, \tag{2}$$

with ε_0 the permittivity of free space, λ_{Di} the ion Debye length, $f(\kappa) = \kappa^{-3/2}$ for the three-dimensional dust acoustic velocity $C_{\mathrm{DA}}^{\mathrm{3D}}$ [12], $f(\kappa) = (2\pi\kappa^2)^{-1/2}$ for the two-dimensional dust acoustic velocity $C_{\mathrm{DA}}^{\mathrm{2D}}$ [20] and $f(\kappa) = [(\kappa^2 + 2\kappa + 2)\exp(-\kappa)/4\pi\kappa]^{1/2}$ for $C_{\mathrm{DL}}(\kappa \gg 1)$, where $\kappa = d/\lambda_{\mathrm{Di}}$ with d the interparticle distance ($d = (n_d^{\mathrm{3D}})^{-1/3}$, $d = (\pi n_d^{\mathrm{2D}})^{-1/2}$, where n_d^{3D} and n_d^{2D} are three and two-dimensional dust density, respectively). Figure 2 shows the dust acoustic velocity $C_{\mathrm{DA}}^{\mathrm{3D}}$, $C_{\mathrm{DA}}^{\mathrm{2D}}$ and the lattice mode C_{DL} with $Z_d = -4.4 \times 10^4$ and $\lambda_{\mathrm{Di}} = 0.11$ [mm]. It is noted that the measured velocities around $\kappa = 3$–6, with the experimental uncertainties, are reasonably well in agreement with the dust acoustic modes as well as the lattice mode. The mode identification of the observed wave is still to be determined.

Typical examples of the trajectories of the flowing microparticles around the obstacle are shown in Fig. 3(a)–3(c). The microparticles flow from left to right by changing inclination of the device. Each line of the figure is a trace of each microparticle during the exposure time. Faint two straight lines originating from the obstacle are shadows behind the needle irradiated by two thin fan laser lights from the radial directions. The void which has a streamlinelike shape can be seen in the middle of the flow. The potential barrier caused by the obstacle decelerates the flow and almost all the microparticles are excluded from

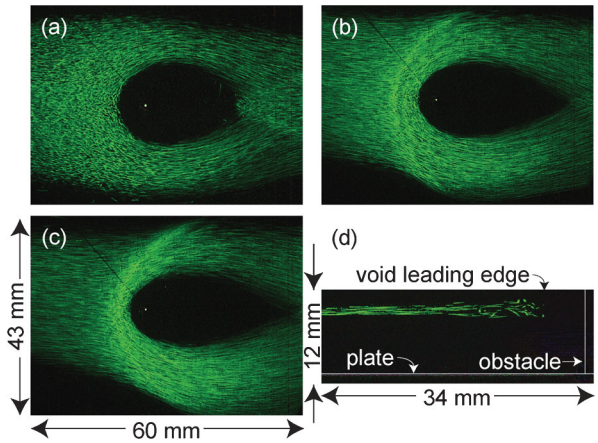

FIG. 3 (color). Typical examples of microparticle flow around a conducting needle [top views: (a)–(c), and side view: (d)]. The needle is shown as a point in the void [(a)–(c)]. The Mach number and velocities are (a) 0.8 (54 ± 8 mm/s), (b) 1.6 (116 ± 24 mm/s), (c) 2.0 (142 ± 29 mm/s), and (d) 1.3 (91 ± 20 mm/s), respectively. The exposure times are 1/10 s for (a)–(c) and 1/20 s for (d). The void structures are characterized by the y-directional spread of (a) 249, (b) 228, and (c) 218 in the unit of the Debye length, respectively.

the area. The trajectories are deflected toward the $\pm y$ direction in front of the void. As was shown in Fig. 3(d) some of the particles in the flow of thin layers move downward in the gravitational direction near the stagnation point in front of the void structure. The lattice structures observed in front of the gate started to deform as propagate in the flow toward the obstacle.

The flow velocity, v_f, in the upstream area has a constant value which is mainly determined by a balance of the gravitational force controlled by the angle θ and the neutral drag force. The flow is almost uniform and there is no prominent structure in the upstream area when v_f is small [Fig. 3(a)]. When v_f increases, an arcuate structure is formed in front of the leading edge of the void [Fig. 3(b)]. The structure can be seen across the flow. For further increase of v_f, a curvature of the arc becomes larger [Fig. 3(c)]. The tail of the void is enlarged with increasing values of v_f.

The arcuate structure is the bow shock. The value of v_f is required to exceed the Mach number 1 when the bow shock is formed. The interparticle distance in the present experiment is 0.42 ± 0.11 mm or $\kappa = 3.8 \pm 1.0$ with the ion Debye length, $\lambda_{\mathrm{Di}} = 0.11$ [mm] when $T_i = 0.1$ [eV] and $n_i = 5 \times 10^{14}$ [m^{-3}]. The value of κ gives the value of velocity 71 mm/s as seen in Fig. 2, which is taken as Mach 1 in the present measurement. The Mach numbers of Figs. 3(a)–3(d) are 0.8, 1.6, 2.0, and 1.3, respectively. It is found that the arcuate structure is distinctive when the flow is supersonic. In addition, there exists a deceleration region between the leading edge of the arcuate structure and the void as shown in Fig. 3(c), that is, there is a region where the flow velocity is reduced in order to keep the flux constant around the obstacle. The presence of such a deceleration region, a subsonic flow region, between the wave front and the stagnation point is one of the defining features of the bow shock [21].

In Fig. 4, the density ratio n_{dp}/n_{d0} is shown as a function of the Mach number, where n_{dp} is the density in front of the stagnation point and n_{d0} is the density of the upstream area. It is known that a polytropic hydrodynamic model provides criterion for the shock wave formation [21]:

$$\frac{n_{dp}}{n_{d0}} = \begin{cases} \left(1+\frac{\gamma-1}{2}M^2\right)^{1/(\gamma-1)} & (M<1) \\ \left(\frac{\gamma+1}{2}\right)^{(\gamma+1)/(\gamma-1)} \frac{M^2}{1+\frac{\gamma-1}{2}M^2}\left(\gamma-\frac{\gamma-1}{2M^2}\right)^{-1/(\gamma-1)} & (M\geq 1) \end{cases}, \tag{3}$$

where γ is the polytropic index. Lines in Fig. 4 are the cases of $\gamma = 5/3$, 2.2, and 3. The experimental results shown by open circles lie between the lines with $\gamma = 5/3$ and $\gamma = 2.2$.

A molecular-dynamics simulation was carried out to examine the formation of bow shock in the flow of microparticles in the presence of potential barrier. A microparticle at a position $\boldsymbol{r}$ produces a potential in a form $\phi(\boldsymbol{r}) = Q\exp(-r/\lambda_D)/4\pi\varepsilon_0 r$, where λ_D is the Debye screening length. To simulate our experiment, microparticles are placed in a plane of 15 cm by 10 cm in the presence of the gravitational force $m_d g \sin\theta$ [15] and an obstacle charge is placed instead of the conducting wire. The density of microparticles is in the range from 100 to 200 particles/cm^2. The equation of motion for the ith particle is $m_d d^2\boldsymbol{r}_i/dt^2 = Q\boldsymbol{E}_i - m_d\boldsymbol{g} - \nu d\boldsymbol{r}_i/dt$, where $i(=1,\ldots,N)$ is the particle number, N the total number of microparticles, $\boldsymbol{E}_i$ the total electric field due to particles surrounding the ith particle, and $\nu = 4\alpha\pi N_n m_n a^2 c_n v/3$ the coefficient of the neutral drag force, where N_n is the neutral density, m_n the neutral mass, c_n the neutral thermal velocity, a the microparticle radius, and v the velocity of the microparticles. The collisional factor α is from 1.4 to 1.5 [15,16].

In Fig. 4 solid circles show the density ratio found in the simulation over a wide range $0 \leq M \leq 3$. A fair agreement with the theory based on Eq. (3) when $\gamma = 2.2$ is found, although small deviation is seen for $M < 1$. The polytropic index found in the simulation and experimental observation may result from the fact that the significant amount of internal energy of the polytropic fluid, which consists of charged microparticles, may be stored in the background plasma. The value of the complex plasma polytropic index indicates that the present complex plasma is far from isothermal ($\gamma = 1$). The polytropic index may be given by the ratio $(C_p + C)/(C_V + C)$, where C_p and C_V are the specific heat coefficients at constant pressure and at constant volume, respectively, and C is the heat capacity. It may be noteworthy to point out that the polytropic index of around 2 is suggested for the study of solar wind [22,23]. The density contour plots for $M = 1.3$ and 2.0 in the

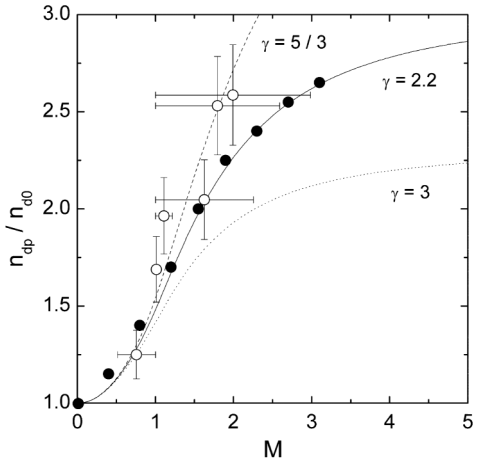

FIG. 4. The density ratio, n_{dp}/n_{d0}, versus Mach number, M. The open circles are the experimental results and the solid circles are the simulation results. The lines are based on Eq. (3) with $\gamma = 5/3$, 2.2, and 3.

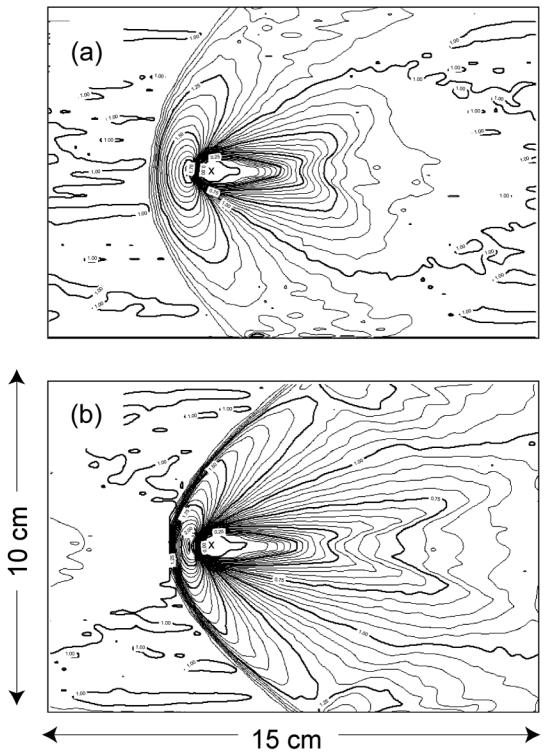

FIG. 5. Simulation results of the density contour plots for Mach numbers (a) $M = 1.3$ and (b) $M = 2.0$. The mark X represents the position of the obstacle charge.

simulation are shown in Fig. 5. It is found that the arcuate structure is formed and its curvature increases with increasing Mach number, which is in agreement with the experimental observation. It is interesting to note that a similar void structure with deflected ions in front of a grain in the presence of supersonic plasma flow was observed in the particle simulation [24].

To summarize our results, the bow shock structure is observed experimentally in the two-dimensional complex plasma system with the supersonic flow of the charged microparticles. The microparticle density at the stagnation in front of the obstacle rises up and the flow pattern forms the arcuate structure when the Mach number exceeds 1. The density ratio between the stagnation point and the regular flow region is measured for a wide range of the flow velocity including subsonic flow and supersonic flow. The dependence of the density ratio on the Mach number is well explained by the polytropic hydrodynamic theory with $\gamma = 1.67 \sim 2.2$ and the molecular dynamics simulation confirms the results. The observed bow shock formation suggests the unique nature of hydrodynamic nonisothermal process involved in a complex plasma.

This work is supported by Asian Office of Aerospace Research and Development under Grant No. AOARD 104158 and JSPS Grant-in-Aid for Scientific Research (A) under Grant 23244110.

[1] V. Nosenko, J. Goree, Z. W. Ma, and A. Piel, Phys. Rev. Lett. **88**, 135001 (2002).
[2] D. Samsonov, J. Goree, H. M. Thomas, and G. E. Morfill, Phys. Rev. E **61**, 5557 (2000).
[3] O. Havnes, F. Li, F. Melansø, T. Aslaksen, T. W. Hartquist, G. E. Morfill, T. Nitter, and V. Tsytovich, J. Vac. Sci. Technol. A **14**, 525 (1996).
[4] A. Melzer, S. Nunomura, D. Samsonov, Z. W. Ma, and J. Goree, Phys. Rev. E **62**, 4162 (2000).
[5] S. Gosh, Phys. Plasmas **16**, 103701 (2009).
[6] Q.-Z. Luo, N. D'Angelo, and R. L. Merlino, Phys. Plasmas **6**, 3455 (1999).
[7] V. Nosenko, S. Zhdanov, and G. E. Morfill, Phys. Rev. Lett. **99**, 025002 (2007).
[8] N. F. Ness, C. S. Scearce, and J. B. Seek, J. Geophys. Res. **69**, 3531 (1964).
[9] G. E. Morfill, H. M. Thomas, U. Konopka, H. Rothermel, M. Zuzic, A. Ivlev, and J. Goree, Phys. Rev. Lett. **83**, 1598 (1999).
[10] S. V. Vladimirov, V. N. Tsytovich, and G. E. Morfill, Phys. Plasmas **12**, 052117 (2005).
[11] E. Thomas, Jr., K. Avinash, and R. L. Merlino, Phys. Plasmas **11**, 1770 (2004).
[12] C. O. Thompson, N. D'Angelo, and R. L. Merlino, Phys. Plasmas **6**, 1421 (1999).
[13] O. Ishihara, J. Phys. D **40**, R121 (2007).
[14] G. E. Morfill and A. Ivlev, Rev. Mod. Phys. **81**, 1353 (2009).
[15] Y. Nakamura and O. Ishihara, Rev. Sci. Instrum. **79**, 033504 (2008).
[16] P. S. Epstein, Phys. Rev. **22**, 710 (1923).
[17] P. K. Shukla and A. A. Mamun, *Introduction to Dusty Plasma Physics* (Institute of Physics Publishing Ltd., London, 2002) Chap. 3, p. 70.
[18] Y. Nakamura and O. Ishihara, Phys. Plasmas **16**, 043704 (2009).
[19] I. Alexeff, W. D. Jones, K. Lonngren, and D. Montgomery, Phys. Fluids **12**, 345 (1969).
[20] G. J. Kalman, P. Hartmann, Z. Donkó, and M. Rosenberg, Phys. Rev. Lett., **92**, 065001 (2004); Z. Donkó, G. J. Kalman, and P. Hartmann, J. Phys. Condens. Matter **20**, 413101 (2008).
[21] L. D. Landau and E. M. Lifshitz, *Fluid Mechanics* (Butterworth-Heinemann, Oxford, 2002), Chap. 12–13, p. 435.
[22] J. A. Newbury, C. T. Russel, and G. M. Lindsay, Geophys. Res. Lett. **24**, 1431 (1997).
[23] I. I. Roussev, T. I. Gombosi, I. V. Sokolov, M. Velli, W. Manchester IV, D. L. Dezeeuw, P. Liewer, G. Toth, and J. Luhman, Astrophys. J. **595**, L57 (2003).
[24] W. J. Miloch, S. V. Vladimirov, H. L. Pecseli, and J. Trulsen, Phys. Rev. E **77**, 065401 (2008); New J. Phys. **11**, 043005 (2009).